

Surface extended-x-ray-absorption-fine-structure study of oxygen interaction with Al(111) surfaces

J. Stöhr, L. I. Johansson, S. Brennan, M. Hecht, and J. N. Miller

Stanford Synchrotron Radiation Laboratory, Stanford University, Stanford, California 94305

(Received 2 November 1979)

We have investigated the oxidation of Al(111) surfaces by means of polarization-dependent surface extended-x-ray-absorption-fine-structure (EXAFS) measurements. The experiments were performed above the oxygen K absorption edge (~ 535 eV) using the total electron-yield detection technique. The oxidation range from monolayer chemisorption corresponding to an ordered oxygen (1×1) overlayer to the formation of a thick surface layer of amorphous oxide has been studied. For the chemisorbed monolayer ($100\text{--}150\text{-L O}_2$) we find a strong polarization dependence of the EXAFS signal which allows the determination of the O–O intraoverlayer separation 2.90 ± 0.05 Å. The O–Al chemisorption bond length has been determined to be 1.79 ± 0.05 Å. Within experimental error we find the same O–Al distance for the initial oxide-like phase which accompanies the chemisorbed phase. At higher exposures (1000-L O_2) the vanishing low-energy-electron-diffraction pattern is accompanied by an increase in the O–Al bond length (1.88 ± 0.03 Å). This value is also observed for heavily oxidized surfaces. The O K edge shows the formation of a strong “white-line”-like threshold resonance with increasing oxygen exposure. This resonance is attributed to transitions to localized final states in Al_2O_3 -like molecular units. It is pointed out that detailed analysis of the absorption threshold may by itself provide information on the local structure of surface complexes. Models for the progressive oxidation process of Al(111) surfaces implied by our data are discussed.

I. INTRODUCTION

The interaction of oxygen with aluminum surfaces is a textbook example of protective oxide formation at metal surfaces. The properties of the surface oxide layer have important industrial implications, for example, for the bonding of aluminum parts in the airplane industry.¹ From an academic point of view the oxygen-aluminum system is of interest because the bonding is of simple s - p character thus enabling *ab initio* theoretical model calculations. In the past such calculations have in fact been carried out using a variety of theoretical techniques^{2–6} for the earliest stages of oxidation, i.e., the chemisorption of oxygen on clean Al surfaces. The present paper attempts to yield structural information on the O–Al surface complexes formed with progressive exposure of the clean Al(111) surface to oxygen and represents a more comprehensive and detailed study than reported previously in form of a letter.⁷

The oxygen-aluminum system in general^{8–13} and the oxygen on Al(111) surface, in particular,^{14–20} have been investigated by numerous experimental techniques. Photoemission studies¹⁶ revealed two distinct phases for the initial interaction of oxygen with Al(111) as evident from different shifts of the Al $2p$ core line. At small oxygen exposures ≤ 100 L ($1 \text{ L} = 10^{-6}$ Torr sec) an ordered (1×1) configuration was found corresponding to an Al $2p$ chemical shift of 1.4 eV. Photoemission^{16,18,19} and

low-energy-electron-diffraction (LEED)^{14,16,20} studies revealed that oxygen chemisorbs in the threefold hollow site on the Al(111) surface with no Al atom in the second Al layer underneath. This site was also favored by theoretical calculations.² Work function measurements^{15,17} imply that around monolayer coverage ($\sim 100\text{--}150\text{-L O}_2$) the O atoms are outside the surface. The second phase corresponds to an Al $2p$ shift of 2.7 eV which is the same value as for bulk Al_2O_3 relative to clean Al.²¹ Thus this phase has been associated with bulklike oxide formation where O atoms penetrate through the surface Al layer.

For the chemisorption stage the O–Al bond length R (or equivalently the oxygen distance Z above the surface) has so far escaped an accurate determination. In all theoretical calculations Z is treated as an adjustable parameter and, depending on the nature of the calculation or the minimization criterion used, widely different Z values have been reported. Lang and Williams² obtained $Z = 1.75$ Å by minimizing the total system energy of a simple atom-jellium model and $Z = 1.32$ Å when Al pseudopotentials were included to first order.⁹ Salahub, Roche, and Messmer⁶ carried out a self-consistent-field $X\alpha$ scattered-wave molecular-orbital calculation for oxygen on an Al(111) cluster and compared the calculated valence bands to the photoemission spectra of Flodström *et al.*¹⁶ Within the accuracy limits of theory and experiment agreement was found for $0.5 \leq Z \leq 1$ Å.

A more direct extraction of geometrical informa-

tion for ordered (periodic) surface complexes can be made from LEED intensity measurements.²² Recently, a dynamical (multiple-scattering) LEED analysis of oxygen on Al(111) spectra recorded at monolayer coverage (~ 150 L) has been reported yielding $Z = (1.33 \pm 0.08) \text{ \AA}$ or $R = (2.12 \pm 0.05) \text{ \AA}$.²⁰ This LEED value is in good agreement with that obtained from the jellium-plus-pseudopotential calculation⁹ but disagrees with the conclusions drawn from the more sophisticated self-consistent $X\alpha$ calculation.⁶ Here we present the results of a surface extended-x-ray-absorption-fine-structure (EXAFS) study of the O-Al system. Our measurements which were carried out in the surface sensitive electron-yield detection mode²³⁻²⁵ reveal an O-Al chemisorption bond length of $R = (1.79 \pm 0.05) \text{ \AA}$ which corresponds to a Z value of $0.70(+0.10, -0.15) \text{ \AA}$. This value is in gross disagreement with the LEED value but strongly supports the conclusions drawn from the self-consistent field $X\alpha$ calculation⁶ and valence-band photoemission data.¹⁶

We have also investigated the oxidelike phase corresponding to an Al $2p$ chemical shift of 2.7 eV.¹⁶ Around monolayer coverage we find the same O-Al bond length for this phase as for the chemisorbed phase. At higher coverage (1000 L O_2 plus heat) the vanishing LEED (1×1) spot pattern is accompanied by an increase in the O-Al bond length ($R = 1.88 \text{ \AA}$). This distance remains the same for a heavily oxidized surface which was exposed to air. We suggest that the oxide phase has a spinel-like structure similar to that of $\gamma\text{-Al}_2\text{O}_3$ (Ref. 26) with an increase of the O-Al bond length as the surface becomes disordered.

We also discuss and analyze the "white-line" fine structure of the O $K(1s)$ absorption threshold. The oxygen exposure-dependent spectra are discussed in terms of theoretical models which account for the existence of strong absorption resonances near the absorption edge. So far calculations have only been carried out for molecules^{27,28} but our studies indicate that analysis of the threshold resonances may yield valuable information on the local structure of surface complexes. Thus we hope to stimulate theoretical investigations of the absorption threshold structure as a function of adsorbate-substrate geometries.

The structure of the present paper is as follows. Section II gives experimental details. Experimental results for the fine structure and EXAFS spectra are given in Sec. III. Here we also compare partial with total electron-yield measurements.²⁹ The data are analyzed and discussed in Sec. IV and structural models for the progressive oxidation of Al(111) are presented. The paper is summarized in Sec. V.

II. EXPERIMENTAL DETAILS

Experiments were performed on the grasshopper monochromator branch line³⁰ of Beam Line I at the

Stanford Synchrotron Radiation Laboratory (SSRL). For the present measurements a 1200 l/mm holographic grating had been installed. The sample chamber consisted of a Vacuum Generators ADES 400 photoemission instrument which operated at a base pressure of 1×10^{-10} Torr.

The Al(111) crystal face was oriented to $\pm 0.5^\circ$ by the Laue backreflection method, polished to $1 \mu\text{m}$ on a diamond wheel and then electropolished. The surface was cleaned *in situ* by cycles of Ar^+ bombardment and annealing to 400°C . The clean and oxygen exposed surface was characterized by core level photoemission spectra and LEED. The Al crystal could be rotated by 360° about a vertical and by 180° about a horizontal axis (see Fig. 1). The x-ray beam was incident on the crystal at an angle θ from the surface with the electric field vector \vec{E} , the sample normal and the [110] direction in the (111) crystal surface all lying in the horizontal plane. We also recorded spectra for an oxidized polycrystalline Al sample which had been exposed to air and single-crystal and polycrystalline bulk Al_2O_3 (corundum). Al_2O_3 has an accurately known O-Al bond length.³¹

The electron-yield detector and its orientation relative to the sample are shown in Fig. 1. The detector consists of a conventional spiraltron electron multi-

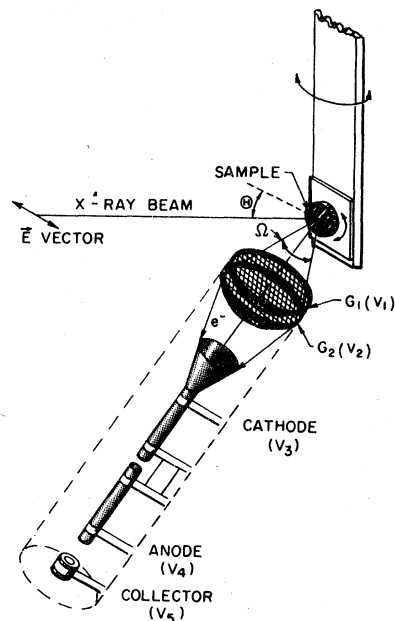


FIG. 1. Experimental geometry of the x-ray beam, the sample, and the electron-yield detector. The x rays are incident at an angle θ from the sample surface. θ is also the angle between the horizontal \vec{E} vector and the sample normal. The sample is rotatable about a vertical and a horizontal axis. The detector consists of two high-transmission grids G_1 and G_2 and a spiraltron electron multiplier.

plier (Galileo model SEM 4219) and two electrically isolated hemispherical metal grids of 2.5-cm radius (Physical Electronics) which are all enclosed by a stainless-steel housing. The detector could be moved *in situ* (~ 2 -cm translation and $\pm 10^\circ$ in angle) by means of a stainless-steel bellow in a gimbal-type mount. Typical operation voltages for the spiraltron were $V_3 = +250$ V, $V_4 = +2500$ V, and $V_5 = +2600$ V. The grids were operated at ground (G_1) and $V_2 = -360$ V (G_2) for the partial yield (PY) and $V_1 \approx +20$ V and $V_2 \approx +30$ V for the total yield (TY) measurements. The solid angle of acceptance Ω of the detector is about the same as for the commonly used Physical Electronics cylindrical mirror analyzer (CMA).³² The detector was operated using pulse counting electronics with typical count rates in the $(0.5-1) \times 10^5$ counts/sec range for the TY measurements. We note that at higher count rates it would be advantageous to measure the output *current* as discussed previously.³³

Normalization of the EXAFS spectra with respect to the incident photon flux was accomplished by dividing the spectra recorded for the oxidized ("dirty") surface by those recorded for a clean surface. As discussed previously^{29,34} this procedure relies on the stability of the electron beam in the storage ring SPEAR. In the final analysis only those spectra were used which fulfilled a consistency criterion. We demanded that the ratio of spectra (individual data sets) be structureless which were recorded for the same sample and polarization direction. The final spectra for the "dirty" and clean surface consisted of about 30 individual sweeps of approximately 10-min duration, respectively. The ratio of the summed "dirty" by the clean spectra is referred to as a *normalized* electron-yield spectrum. For the final analysis of the spectra a background due to pre-edge absorption processes was subtracted by extrapolating the pre-edge absorption to energies above the O K edge.

III. EXPERIMENTAL RESULTS

A. Partial yield versus total yield

The principles of the various electron-yield detection techniques have been discussed before.^{23,29,35} For low- Z atoms the Auger detection mode²³ cannot be used because of strong interferences with the elastic photoemission signal.^{29,36} This is why previous surface EXAFS measurements in the soft x-ray region^{24,29,34,36,37} relied on the detection of inelastically scattered electrons. Recent measurements of oxygen on GaAs(110) (Ref. 37) indicated that the highest surface sensitivity is achieved if only electrons of kinetic energy $E_k \geq 300$ eV are detected. The analyzer window setting for this partial-yield detection mode and for the oxygen on the Al system of interest is

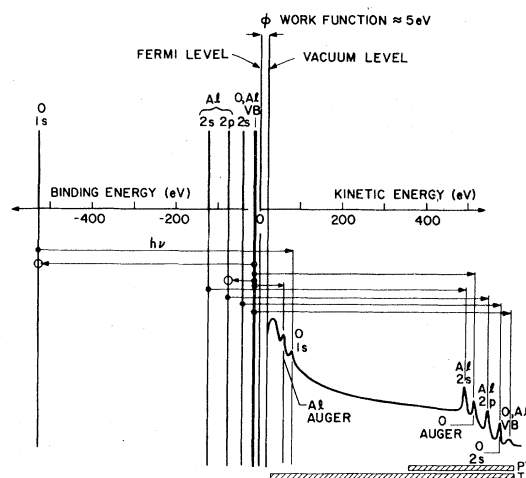


FIG. 2. Energy-level diagram and photoemission spectrum at a photon energy $h\nu$ for a hypothetical sample consisting of O and Al atoms. Window settings for the partial-yield (PY) and total-yield (TY) detection modes are indicated in the lower right half.

illustrated in Fig. 2. Here we indicate on the left side all core level binding energies of the O-Al system and on the right side all transitions and the resulting photoemission spectrum at a photon energy $h\nu$. The lower kinetic energy limit of the partial-yield window is chosen as high as possible but low enough such that at the O 1s threshold ($h\nu \approx 530$ eV) all photoemission peaks corresponding to lower binding-energy core levels are included in the PY window. For the O-Al system we used a low-energy cutoff of 360 eV. This was accomplished by applying a retarding voltage $V_2 = -360$ V to the second detector grid G_2 (see Fig. 1) while operating G_1 at ground potential. For the total yield (TY) spectra all electrons emitted from the sample were collected. This is done most efficiently by operating G_1 and G_2 at small positive potentials.

For a given sample the detection mode yielding the highest *signal-to-noise* ratio should be chosen. Let N be the total and N_0 be the background count rate (obtained from extrapolation of the pre-edge region) at a photon energy above the O K absorption edge ("dirty" sample). Then the *signal-to-noise* ratio to be maximized is given by $S_N = (N - N_0)/\sqrt{N}$. For small *signal-to-background* ratios [$S_B = (N - N_0)/N_0 < 1$] we obtain $S_N = S_B\sqrt{N}$. Normalized electron-yield spectra for a sample of 100-L O₂ on Al(111) in the region of the O K edge are shown in Fig. 3. The *signal-to-background* ratio at the O K edge is $S_B = 8.5\%$ for the total- and $S_B = 17.5\%$ for the partial-yield spectra. The total electron count rate N was a factor of 15 higher for the TY detection mode. Thus in the present case the *signal-to-noise* ratio for the TY mode is about a factor of 2 larger than for the

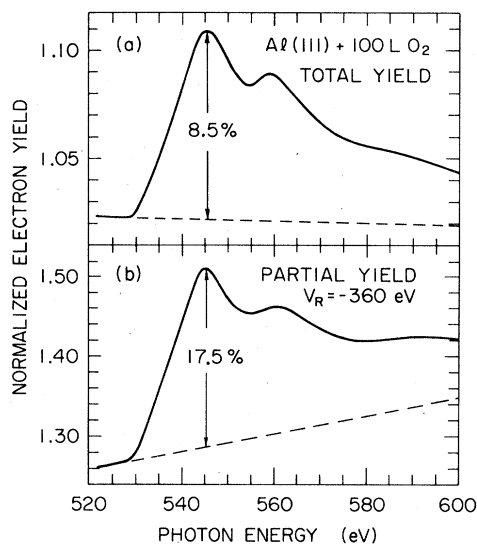


FIG. 3. Comparison of surface EXAFS spectra taken around the O K edge in the total- and partial-yield detection mode for about a monolayer of oxygen on Al(111). The pre-edge background extrapolated past the K edge is shown as a dashed line. The partial-yield spectrum exhibits a two times higher signal-to-background ratio than the total-yield spectrum but the count rate was lower by a factor of 15. Spectra were recorded at $\theta = 11^\circ$.

PY mode, although the later exhibits a higher signal-to-background ratio (i.e., surface sensitivity). All spectra discussed below were recorded using the TY technique.

B. Absorption spectra

The fine structure around the O K edge is shown in Figs. 3 and 4 for various oxidation stages. The largest threshold effect is the intensity variation of peak X with oxygen exposure as evident from Fig. 4. In the range of monolayer coverage (100–150-L O_2) the intensity of peak X is comparable to that of the EXAFS structures Y and Z while it is very pronounced at higher oxygen coverage. A more quantitative picture is obtained if we compare the height of peak X to the height of the atomic absorption step at the O K edge. For this purpose we extrapolate the average absorption above the edge down to the K -edge jump as indicated by the dashed lines in Fig. 4. If γ_0 is the value of the dashed line and γ the peak value of X at 546 eV the quantity $S = (\gamma - \gamma_0)/\gamma_0$ provides a measure for the relative intensity of the “white-line” threshold structure X . We obtain $S = 45\%$, 30% , and 15% for the spectra from top to bottom in Fig. 4. As expected the strength of the total oxygen absorption signal (edge jump in Fig. 4) varied with exposure but was independent of θ . We observed the values $S_B \sim 6\%$ (100 L), $\sim 8.5\%$

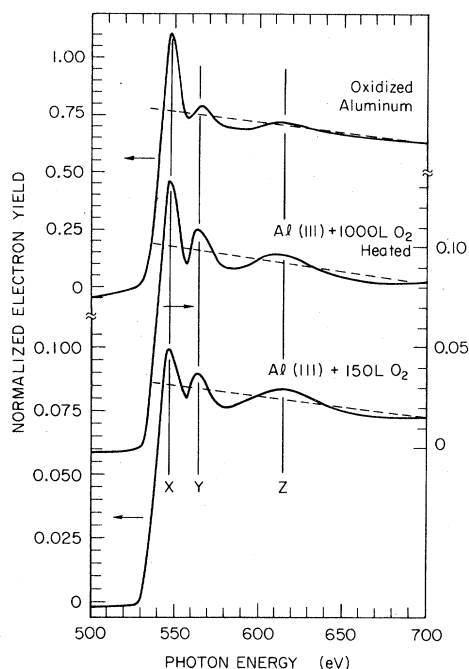


FIG. 4. Fine structure around the O K edge as a function of oxygen exposure. The top spectrum was recorded on a polycrystalline sample exposed to air. The dashed line indicates the “atomic” absorption above threshold. Peak X is the “white-line” threshold peak and peaks Y and Z are EXAFS-related structures. The intensity of peak X relative to the atomic absorption step was independent of the \vec{E} vector orientation θ .

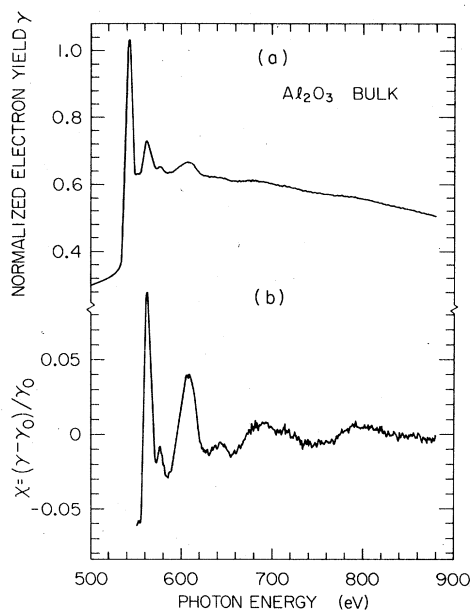


FIG. 5. (a) Oxygen K -edge absorption spectrum of bulk Al_2O_3 recorded for a sample of Al_2O_3 powder which was deposited by means of sedimentation on clean copper. (b) EXAFS structure above the O K edge after background subtraction.

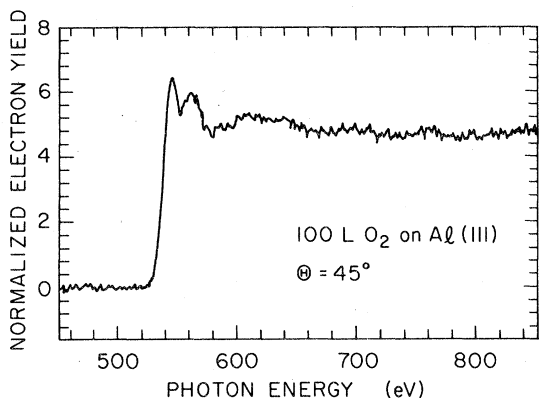


FIG. 6. Normalized electron-yield EXAFS spectrum for 100-L O_2 on Al(111) recorded at $\theta = 45^\circ$. Note that the signal-to-background ratio is only about 6% at the O K edge.

(150 L), $\sim 10\%$ (1000L), and $\sim 75\%$ (oxidized Al) for the signal-to-background ratios just above the K edge, respectively.

Figures 5(a) and 6 show normalized EXAFS spectra for the most concentrated (bulk Al_2O_3) and the most dilute [100-L O_2 on Al(111)] samples studied. The oxygen dilution ratio is directly reflected by the signal-to-noise ratio of the spectra. For the bulk Al_2O_3 spectrum we also show the EXAFS oscillations obtained after background subtraction in Fig. 5(b).

IV. DATA ANALYSIS AND DISCUSSION

A. Near edge structure

The fine structure at the absorption threshold in solids has long been of interest for a variety of reasons. Besides studies of excitonic and many-body effects³⁸ which concentrate on the structure within 1–2 eV above threshold recently there has been a revived interest in the so-called “white-line” threshold structures.^{39–41} White lines are strong absorption resonances typically within the first 20 eV above the absorption threshold. In the past white lines have been mainly discussed for the $L_3(2p_{3/2})$ and $L_2(2p_{1/2})$ transition-metal edges. Their strength has been correlated with the d -like density of states above the Fermi level and a large $p \rightarrow d$ dipole matrix element.^{39–41} Previous studies on the K edges of low- Z atoms have also revealed intense white-line threshold structures in almost all cases investigated.^{24, 29, 35, 36} In the following we shall discuss this phenomenon in general and for the oxygen-on-Al system in particular.

Strong absorption resonances occur if *final states* of the symmetry allowed by dipole selection rules are available and a strong *overlap* exists between initial- and final-state wave functions (i.e., a large transition

matrix element). For L_2 or L_3 edges the above criteria are met for many solids with d -like conduction-band states. Because of the localized nature of the latter large cross sections result. For K or L_1 edges final states of p -like character are important which are in general less localized than d -like states. Hence, even if p -like final states are available one would not in general expect a strong resonancelike behavior.

For molecules Dehmer²⁷ has discussed cases where strong resonances exist above the K absorption threshold. If the central atom forms polar bonds with two or more electronegative neighbor atoms a two-well potential may result.²⁷ The inner potential well arises from the partially screened nucleus of the central atom. The outer well is due to the Coulomb attraction which an electron experiences at large distance by the molecular ion. The two wells are separated by a potential barrier which is caused by the electronegative neighbor atoms. States located in the inner well are “bottled up” by the effective pseudopotential barrier and will thus overlap significantly with core states of the central atom. Thus strong transitions are expected between initial-core and inner-well final states. Transitions to outer-well final states will be weaker due to smaller wave-function overlap.

The localized final states in the cases discussed above are a consequence of the *pseudopotential* barrier set up by the electronegative neighbor atoms. Dehmer and Dill²⁸ have shown that resonances above the K -shell threshold in molecules should exist on more general grounds. These so-called “shape resonances” have their origin in the *molecular field* which couples the dipole allowed p -wave electron to the entire range of angular momentum states contributing to the allowed σ - and π -ionization channels. In addition, the spatial extent of the molecular field may support resonant penetration of high- l partial waves through their centrifugal barrier into the molecular core. These two circumstances combine to produce a dramatic enhancement of the photoelectron cross section. Both highly *localized* (discrete shape resonances) as well as *quasibound* (continuum resonances) final states are possible. The existence of such resonances should be a very general phenomenon with the resonance strength depending on the spacial extent and symmetry of the molecular field.

The effects discussed above for *molecules* should also be present in solids,^{27, 42} in particular, *surface complexes* which locally often resemble molecular units. Recently Bianconi, Bachrach, and Flodström⁴³ interpreted the oxygen induced changes of the Al $L_{2,3}$ fine structure for the Al(111), (100), and (110) low-index faces in terms of Dehmer's²⁷ double-well pseudopotential barrier model. With increasing oxygen exposure Bianconi *et al.* found the development of strong resonances within the first 15 eV above the Al $L_{2,3}$ threshold. These resonances

were attributed to inner-well final states in the microscopic structural unit of oxide formed by the positive Al ion surrounded by the electronegative O ions. Within this model the increase in resonance strength with oxygen coverage is directly related to the increasing *ionicity* of the O–Al bond as evident from the growing chemical shift of the Al 2*p* photoemission line.^{8,16} As the bond ionicity increases, a potential barrier is formed due to negative charge compilation on the oxygen atoms and the states in the resulting inner well give rise to the enhanced absorption above threshold.

As shown in Fig. 4 the O *K* edge exhibits the same resonance behavior with increasing oxygen exposure as the Al *L*_{2,3} edge. This is not necessarily expected because different initial- and final-state wave functions are involved. In particular, we are now probing excitations on the electronegative O rather than the electropositive Al atom. If we maintain the two-well potential picture used above to explain the Al *L*_{2,3}-edge effects we are led to the remarkable conclusion that O 1*s* electrons are excited into inner-well states inside the molecule rather than into outer-well states. This indicates that the outer well is located beyond the O nuclei. Similar behavior was found for SF₆ where resonance absorption was observed both above the *L*_{2,3} edge of the electropositive S and the *K* edge of the electronegative F atoms.²⁷ As discussed by Dehmer²⁷ inner-well states of *s*, *p*, and *d* symmetry are available in the tetrahedral or octahedral environment expected for an Al₂O₃-like molecular complex. Thus transitions from *s* or *p* initial-core states are allowed. This is an agreement with the Al *L*_{2,3}- and *K*-edge spectra for Al₂O₃ which both show a white-line threshold structure.⁴⁴

At present it cannot be excluded, however, that the observed threshold enhancement for oxygen on Al is due to a shape resonance. In this picture changes in the threshold structure are expected because the local *structure* of the O–Al surface complex changes with O exposure. Because shape resonances arise from final-state scattering effects the strength of the resonance might be expected to increase as the central atom is caged in by more neighbor atoms. This would also explain the observed threshold variations.

In order to better understand the observed threshold effects it is clearly desirable that model calculations be carried out. A detailed understanding of the observed effects would allow us to discriminate between the two suggested theoretical models. More important, it might be possible to obtain *structural information* on surface complexes from analysis of the absorption edge structure alone.

B. Theoretical EXAFS model

In the case of *K*-shell absorption the EXAFS signal

is given by^{45,46}

$$\chi(k) = \frac{\gamma - \gamma_0}{\gamma_0} = - \sum_i A_i(k) \sin[2kR_i + \phi_i(k)] \quad (1)$$

where *i* designates a neighbor shell at a distance *R_i* from the absorbing atom. The wave vector *k* (Å⁻¹) is related to the energy (eV) by the relation

$$k = 0.5123(h\nu - E_0 - \Delta)^{1/2} \quad (2)$$

where *hν* is the photon energy, *E₀* is the energy at the *K*-edge inflection point, and Δ is an adjustable parameter.^{47,48} The total phase shift $\phi_i(k)$ represents⁴⁷ the sum of the phase shifts for the backscattering atom and the central absorbing atom. When the neighbor shell consists of identical atoms, the total EXAFS amplitude *A_i(k)* is given by

$$A_i(k) = (N_i^*/kR_i^2) F_i(k) e^{-2\sigma_i^2 k^2} e^{-2R_i/\lambda(k)} \quad (3)$$

where *F_i(k)* is the backscattering amplitude. The two exponential terms are a Debye-Waller-factorlike term and a damping term due to inelastic scattering of the photoelectrons.

The most important parameter in *polarization-dependent* surface EXAFS measurements is the effective coordination number *N_i** in Eq. (3) which is given by⁴⁹

$$N_i^* = 3 \sum_{j=1}^{N_i} \cos^2 \alpha_j \quad (4)$$

The sum is over all atoms *j* (total number *N_i*) in the *i*th neighbor shell and α_{*j*} is the angle between the electric field vector \vec{E} and the position vector \vec{r}_{ij} from the central atom to the *j*th atom in the *i*th shell. Equation (4) tells us that a neighbor atom *j* only contributes to the EXAFS signal if the \vec{E} vector has a sizable component along its position vector \vec{r}_{ij} . For inherently anisotropic systems like surfaces the polarization dependence of the EXAFS signal therefore provides an extremely powerful tool to sort out neighbor atoms which are located in different directions from the central atom.^{50,51} In fact, the \vec{E} vector can be envisioned as a “search light” revealing all neighbors in a given direction. We shall make use of this concept later.

For atoms chemisorbed in ordered configurations on single-crystal surfaces Eq. (4) has to be evaluated for an assumed model geometry and a given experimental \vec{E} -vector orientation.²⁹ In many cases only the (polar) \vec{E} -vector orientation with respect to the surface normal needs to be considered since the symmetry of the atoms in the surface plane eliminates any azimuthal dependence of *N_i**. The threefold hollow chemisorption site on a (111) surface is an example and we shall discuss it in the following.

The case of an oxygen atom chemisorbed in the threefold hollow site on an Al(111) surface is illustrated in Fig. 7. Here θ is the angle between the sur-

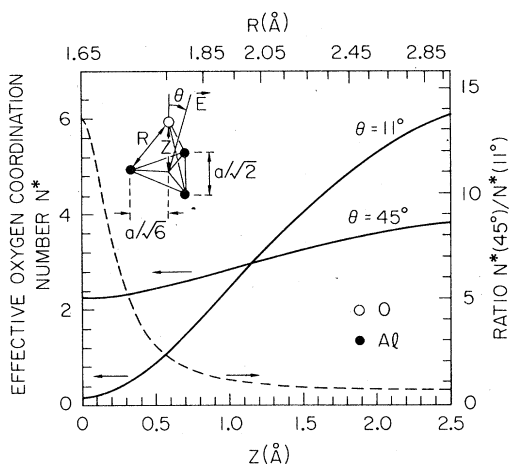


FIG. 7. Calculated effective oxygen coordination number N^* as a function of the O-Al distance R and the O distance Z above the Al surface for O chemisorbed in the threefold hollow site on Al(111) [Eq. (5)]. The assumed geometry is also shown. Calculations were carried out for the two experimental cases $\theta = 11^\circ$ and $\theta = 45^\circ$.

face normal and the electric field vector and Z is the oxygen distance above the Al surface layer. $R = (\frac{1}{6}a^2 + Z^2)^{1/2}$ is the O-Al bond length where $a = 4.04 \text{ \AA}$ is the Al fcc lattice constant.⁵² Evaluation of Eq. (4) yields

$$N^* = \frac{9}{(\frac{1}{6}a^2) + Z^2} \left[\frac{a^2}{12} \sin^2\theta + Z^2 \cos^2\theta \right]. \quad (5)$$

Thus, whether and how N^* varies with θ depends on the actual position Z of the oxygen atom. For a distance $Z = \frac{1}{6}a\sqrt{3} = 1.17 \text{ \AA}$ (corresponding to $R = \frac{1}{2}a = 2.02 \text{ \AA}$) N^* is isotropic and equal to three. Calculated values for N^* as a function of Z or R are shown in Fig. 7 for our two experimental geometries $\theta = 11^\circ$ and $\theta = 45^\circ$. Also shown in the figure is the ratio between N^* at 45° and 11° .

Besides the chemisorption site considered above there are two other sites of interest for the Al(111) surface. These sites lie between the first and second layer of Al atoms as shown in Fig. 8. As illustrated by Fig. 8(a) two distinctly different hollow sites A and B in the surface Al layer can be distinguished when their orientation with respect to the second Al layer is considered. Underneath site A the second layer exhibits another threefold hollow site which is rotated by 60° with respect to that in the first layer [see Fig. 8(d)]. For site B an Al atom is located in the second layer directly underneath [see Fig. 8(c)]. For the chemisorbed site *outside* the surface layer [Fig. 8(b)] sites A and B are equivalent with respect to the Al *nearest* neighbors. For the oxide phase, however, in which the oxygen atom is assumed to

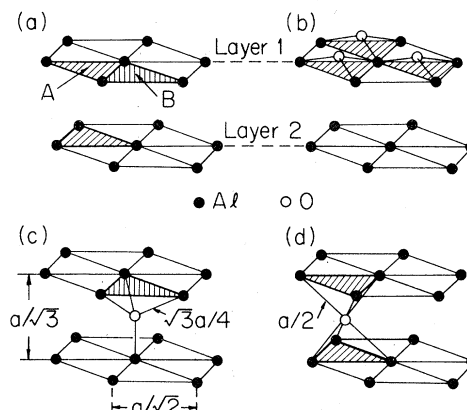


FIG. 8. (a) Model of the first two Al layers for a clean Al(111) surface. Two threefold hollow sites A and B in the first layer can be distinguished with respect to the second layer. Site A has another threefold hollow site underneath while site B is on top of a second-layer Al atom. (b) Proposed geometry of O atoms chemisorbed in a (1×1) configuration on Al(111). Adsorption occurs on site A in positions which are a continuation of the Al lattice (fcc stacking). (c) Ideal tetrahedral O coordination underneath site B . The O-Al bond length is 1.75 \AA . (d) Ideal octahedral O coordination underneath site A . The O-Al bond length is 2.02 \AA .

penetrate through the first layer, sites A and B give different results. As shown in Fig. 8(c) an oxygen atom underneath site B is fourfold coordinated. Placing the O atom at the center of the tetrahedral interstice at $Z = -\frac{1}{12}a\sqrt{3} = -0.58 \text{ \AA}$ yields an O-Al bond length $R = \frac{1}{4}a\sqrt{3} = 1.75 \text{ \AA}$. The *effective* coordination number N^* is isotropic and therefore equal to the *real* coordination number $N = 4$. If the O atom is placed at the center of the octahedral interstice at $Z = -\frac{1}{6}a\sqrt{3} = -1.17 \text{ \AA}$ [Fig. 8(d)] the O-Al bond length is $R = \frac{1}{2}a = 2.02 \text{ \AA}$. The isotropic effective coordination number is $N^* = 6$. Note that this is a special case of Eq. (5).

Finally we discuss the effective coordination number of an O atom in the geometry shown in Fig. 8(b) (i.e., a 1×1 overlayer) with respect to other O atoms in the overlayer. The O-O distance is the same as the Al-Al separation in the surface, i.e., $R_2 = a/\sqrt{2} = 2.86 \text{ \AA}$. Each O is surrounded by six others. N^* is obtained from Eq. (5) setting $Z = 0$ and considering that there are six instead of three neighbors. We obtain

$$N^* = 9 \sin^2\theta. \quad (6)$$

For our two experimental cases we find $N^* = 4.5$ ($\theta = 45^\circ$) and $N^* = 0.3$ ($\theta = 11^\circ$).

C. EXAFS analysis

1. Phase shifts

The accurate determination of neighbor separations by means of EXAFS is dependent on the availability of reliable phase shifts. For high- Z atoms calculated phase shifts have been successfully used to determine nearest-neighbor distances to 0.01–0.02-Å accuracy.⁴⁷ The determination of distances from low- Z atoms by means of EXAFS is at present more difficult. The most important problem is the limited EXAFS energy range available above the low- Z K edge. This is due either to limitations of the presently available monochromators³¹ or the interference of one of the abundant absorption edges below 1000 eV. In most cases a range of less than 400 eV above the K edge is available which corresponds to a wave-vector region of $k \leq 10 \text{ \AA}^{-1}$. This restriction makes the use of calculated phase shifts less reliable since they are most accurate at high- k values ($k > 8 \text{ \AA}^{-1}$) and in many cases unreliable for $k < 4 \text{ \AA}^{-1}$.^{47,50} The problem is enhanced by the fact that nearest-neighbor distances from low- Z atoms are in general shorter than from heavier atoms resulting in fewer EXAFS oscillations per given energy or wave-vector interval.

In the present study we have tried to avoid the uncertainty associated with calculated phase shifts when possible. As an experimental standard for the O–Al phase shift we employed a sample of bulk Al_2O_3 (corundum) for which the O–Al bond length $R = 1.915 \text{ \AA}$ was known from x-ray diffraction.³¹

The EXAFS oscillations for bulk Al_2O_3 as a function of k are shown in Fig. 9(a). We recorded spectra for three different samples of Al_2O_3 : (1) single-crystal corundum, (2) polycrystalline Al_2O_3 powder, and (3) a sapphire sample with a (0001) surface orientation. The spectra showed slightly different absorption structures near the O K -edge threshold ($h\nu < 580 \text{ eV}$) but identical EXAFS at higher photon energies. Analysis of the EXAFS structure yielded identical results for the O–Al nearest-neighbor shell which is evident in the Fourier transform in Fig. 9(b) as the dominant peak around 1.5 Å. Knowing that this peak corresponds to a O–Al bond length of $R = 1.915 \text{ \AA}$ we can derive a scattering phase shift for the O–Al system.²⁹ The derived phase shift using $\Delta = 0$ [see Eq. (2)] is shown in Fig. 10. As observed before for the O–Si and N–Si phase shifts the O–Al phase shift is very closely linear in k and can be expressed as

$$\phi = 3.65 - 0.72k \quad (7)$$

This can be compared to the calculated phase shift by Lee, Boon-Keng Teo, and Simmons⁵³ which in the range $k > 4 \text{ \AA}^{-1}$ can be fitted to the quadratic expression

$$\phi = \phi_0 + \tau_{\text{Al}} = 5.573 - 0.9648k + 0.0251k^2 \quad (8)$$

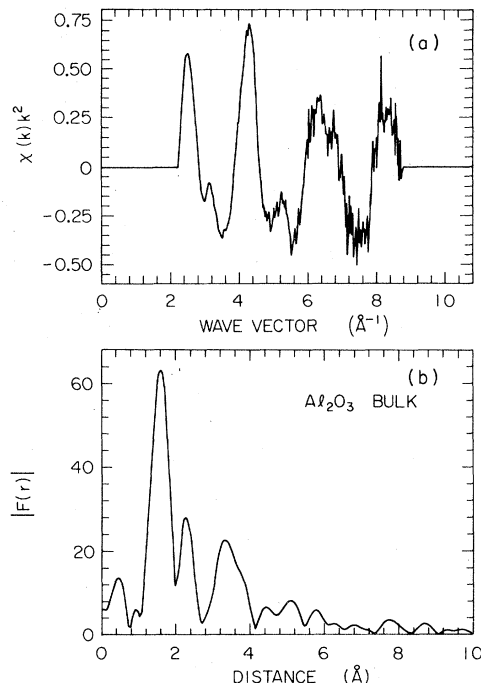


FIG. 9. (a) EXAFS structure as a function of wave vector for bulk Al_2O_3 as shown in Fig. 5. (b) Fourier transform of the signal in Fig. 9(a).

Here ϕ_0 is the total central O atom and τ_{Al} the Al backscattering phase shift. The calculated phase shift was found to yield an approximately 0.05-Å shorter O–Al distance than the experimental one. This is in agreement with our findings for the O–Si system²⁹ where the calculated phase shift underestimated the bond length by 0.03 Å.

Standards to determine the phase shift for the O–O scattering case are more difficult to find since

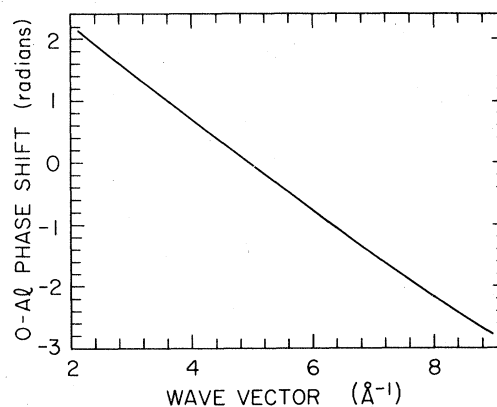


FIG. 10. O–Al phase shift derived from corundum choosing the inflection point of the O K edge as $k = 0$. The phase shift is very nearly linear and can be expressed as $\phi = 3.65 - 0.72k$.

in solids O atoms are usually not surrounded by *first*-nearest-neighbor (NN) O atoms. The use of second-NN O—O distances for a phase-shift determination is considered quite unreliable. In addition to other factors, the signal from second-NN is often quite weak and thus less reliable. We have therefore used a calculated O—O phase shift in our analysis which is given by⁵³

$$\phi = \phi_0 + \tau_0 = 3.419 - 0.960k + 0.0256k^2 \quad (9)$$

2. 100–150-L spectra

The surface EXAFS signal $\chi(k)k^2$ above the O *K*-absorption edge for a sample of 100-L oxygen on Al(111) is shown in Fig. 11 for two polarization directions θ . The shown signals were obtained from the raw data by the data reduction procedures discussed in Ref. 29. The oscillations in Fig. 11(a) ($\theta = 11^\circ$) are very nearly sinusoidal while those in Fig. 11(b) ($\theta = 45^\circ$) exhibit a strong nonperiodic beat frequency. Such behavior is characteristic for systems where more than one neighbor shell contributes to the EXAFS signal. The strong polarization dependence is most clearly evident at wave vectors $k > 6 \text{ \AA}^{-1}$.

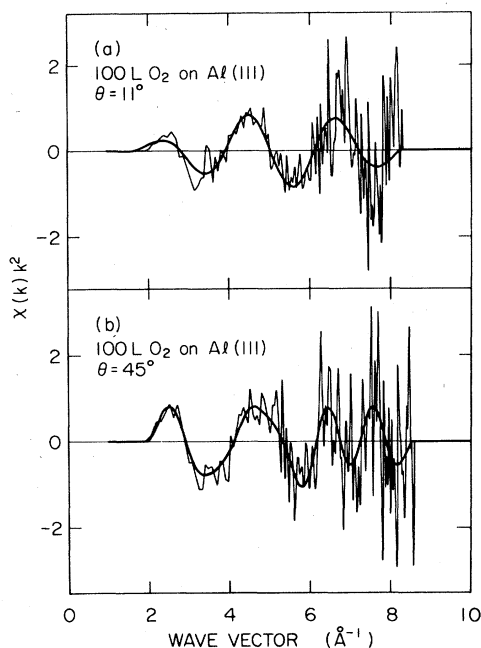


FIG. 11. (a) EXAFS signal $\chi(k)k^2$ above the oxygen *K* edge for a sample of 100-L O₂ on Al(111) and $\theta = 11^\circ$. The noisy signal is the original data. The smooth line represents the main frequency and is the Fourier filtered signal corresponding to peak *A* in Fig. 11(a). (b) Same as in Fig. 11(a) for $\theta = 45^\circ$. The smooth line represents the two superimposed dominant frequencies corresponding to the Fourier filtered nearest-neighbor peaks *A* and *B* in Fig. 11(b).

The Fourier transforms of the noisy EXAFS signals $\chi(k)k^2$ in Fig. 10 are shown as solid lines in Fig. 12, respectively. Also shown as a dashed line in Fig. 12(b) is the transform of the EXAFS oscillations $\chi(k)k^3$ which enhances the contribution from the high-*k* region of the signal. Thus the differences between the two signals in Figs. 11(a) and 11(b) become more apparent. The transform for $\theta = 11^\circ$ in Fig. 12(a) is dominated by a single peak *A*. This peak is also observed for $\theta = 45^\circ$. In addition, for this polarization a second strong peak *B* is observed which for the $\chi(k)k^3$ weighted signal has almost the same intensity as peak *A*. The transforms for a slightly higher oxygen exposure of 150 L look very similar as those in Fig. 12 except that for the $\theta = 45^\circ$ case peak *B* becomes about 30% weaker with respect to peak *A*. We have filtered out peaks *A* in Fig. 12(a) and peaks *A* plus *B* in Fig. 12(b) and back-transformed them into *k* space. The so-obtained filtered EXAFS signals are shown as smooth solid lines in Fig. 11, respectively.

Peak *A* is attributed to the nearest-neighbor O—Al distance *R* (see Fig. 7). We have determined *R* using the experimentally derived phase shift given by Eq. (7) and shown in Fig. 10. The analysis was car-

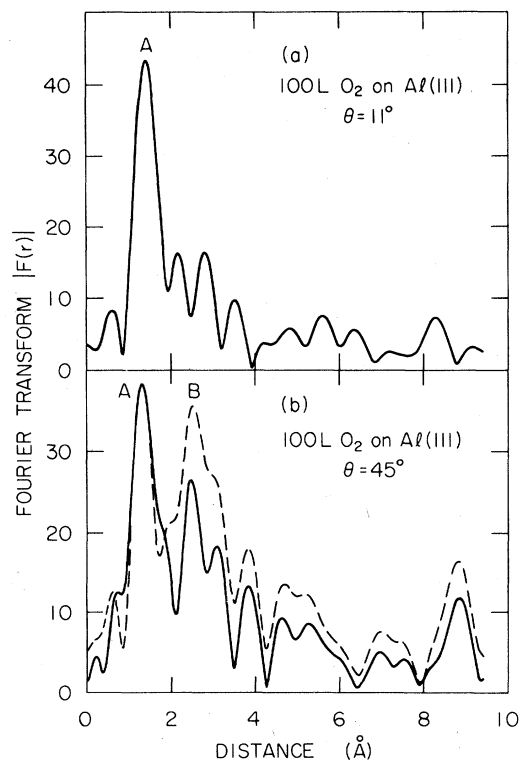


FIG. 12. (a) Absolute value of the Fourier transform $|F(r)|$ of the noisy EXAFS signal in Fig. 10(a). Note that the peaks in $|F(r)|$ are displaced from the true distance by a phase shift. (b) $|F(r)|$ of the noisy signal $\chi(k)k^2$ in Fig. 10(b) (solid line) and of the signal $\chi(k)k^3$ (dashed line).

TABLE I. Derived bond lengths for oxygen on Al(111).

Oxygen exposure (Langmuirs)	θ^a	O-Al distance (\AA)	O-O distance (\AA)
100	11°	1.81 ± 0.03	
100	45°	1.76 ± 0.05	2.90 ± 0.05
150	11°	1.80 ± 0.03	
150	45°	1.81 ± 0.03	2.95 ± 0.10
1000 heated	11°	1.88 ± 0.03	

^aSee Fig. 7.

ried out using both the method proposed by Lee and Beni⁴⁷ and that of Martens *et al.*⁴⁸ The two methods yielded identical results which are summarized in Table I. The obtained distances in the range of monolayer coverage (100–150-L oxygen) all lie within 0.05 \AA . However, the value for 100-L O₂ exposure and $\theta = 45^\circ$ is shorter than the other three. For this case the EXAFS signal [Fig. 11(b)] is more complex and the interference of the signals from the first- and second-neighbor shells [peaks *A* and *B* in Fig. 12(b)] might cause a slight error in the distance determination, especially with the limited *k* range available.

Thus far we have ignored the presence of smaller amounts of an *oxidelike* phase in addition to the *chemisorbed* oxygen on Al(111).¹⁶ As shown in Fig. 13 the two phases are revealed by a chemical shift of the Al 2*p* photoemission line to higher binding energy which is 1.4 eV (peak *B*) for the chemisorbed and 2.7 eV (peak *C*) for the oxidelike state. In fact, the latter phase is called “oxidelike” because its chemical shift relative to clean Al (peak *A* in Fig. 13) is the same as for Al₂O₃.²¹ In the monolayer coverage range (100–150-L O₂) the oxide phase cannot be avoided and we find that the Al 2*p* photoemission intensity corresponding to the oxide phase is at least one-third of the intensity corresponding to the chemisorbed phase. If we assume that for the oxide formation the O atoms penetrate through the surface layer [as, for example, in Figs. 8(c) and 8(d)] the first two Al layers or twice as many Al atoms are affected for a given number of O atoms as for the chemisorbed phase above the surface. Thus if we assume an intensity ratio of 2 between the 1.4 eV and 2.7 eV shifted Al 2*p* core lines we expect about four times as many O atoms in the chemisorbed than in the oxide phase. The relative contribution of the two kinds of differently coordinated O atoms to the EXAFS signal also depends on the effective coordination number *N**. Here we shall neglect other dependencies (e.g., Debye-Waller-factor effects) because they are more difficult to assess. In Al₂O₃ each O atom is

coordinated by 4 Al atoms yielding *N** = *N* = 4. This number needs to be compared to the θ -dependent *N** value for O on Al(111) plotted in Fig. 7. For an O–Al distance around 1.8 \AA we obtain *N** ≈ 2.5 for $\theta = 45^\circ$ and *N** ≈ 1.5 for $\theta = 11^\circ$. Since the number of chemisorbed O atoms is about a factor of 4 larger than that of O atoms in the oxide, the former are expected to contribute 2.5 (1.5) times as much to the EXAFS signal. We conclude that the 100 L, 45° *R* value in Table I is the least and the 150 L, 11° value is the most sensitive to a contribution from the oxide phase. The slightly shorter distance *R* = 1.76 \AA obtained at 100-L O₂ exposure and $\theta = 45^\circ$ might therefore be the more accurate value for the O–Al chemisorption bond length. However, since all values lie within 0.05 \AA we conservatively quote a value of (1.79 ± 0.05) \AA for the O–Al chemisorption bond length. As shown in Fig. 7 this value corresponds to a vertical separation of *Z* = 0.7 (+0.10, –0.15) \AA from the outermost plane of Al nuclei assuming chemisorption in the threefold hollow site. In order to explain the insensitivity of the derived *R* value for the nearest-neighbor distance with respect to the angle of

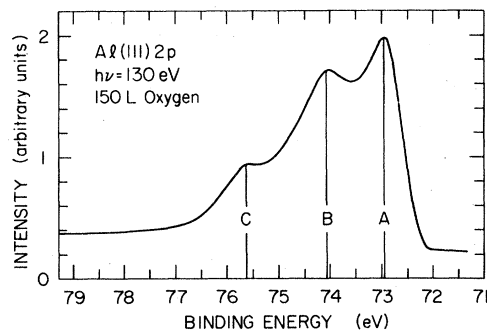


FIG. 13. Al 2*p* photoemission spectrum for 150-L O₂ on Al(111) recorded at $h\nu = 130$ eV. Peak *A* is due to bulk Al atoms, peak *B* to Al atoms which are bonded to chemisorbed oxygen, and peak *C* to Al atoms which are part of local oxidelike units.

incidence and oxygen exposure the O–Al bond length in the oxidelike surface complex has to be the same as for the chemisorbed phase within the error limits quoted above.

Peak *B* is assigned to the O–O distance in the chemisorbed overlayer. Since the oxygen atoms lie in a plane parallel to the surface the O–O distance should only be observable at large- θ values [see Eq. (6)]. It should be negligible at $\theta = 11^\circ$ ($N^* = 0.3$) but significant at $\theta = 45^\circ$ ($N^* = 4.5$), in agreement with the fact that peak *B* is only observed at $\theta = 45^\circ$. While it is clear from the polarization dependence that peak *B* corresponds to a distance between atoms which lie parallel or nearly parallel to the surface plane we still need to examine whether it could be due to O–Al second-nearest-neighbor scattering. For O atoms in the threefold hollow site and a distance of 0.7 Å outside the surface plane the three second-nearest-neighbor Al atoms are 3.37 Å away. Peak *B* falls at a distance around 2.9 Å both using O–O or O–Al scattering phase shifts. We can thus exclude this possibility. We note, however, that the shoulder on the right side of peak *B* in Fig. 12(b) (dashed curve) corresponds to a distance of ~ 3.4 Å and might thus indicate the three Al second-nearest neighbors. Using the calculated O–O phase shift given by Eq. (9) we find peak *B* to correspond to a distance of (2.90 ± 0.05) Å. Here we have used the more reliable value for the 100-L, $\theta = 45^\circ$ case listed in Table I. This value is in excellent agreement with the expected 2.86 Å separation from a given chemisorbed O atom to its six nearest O neighbors in a (1×1) overlayer. We note that the derived distance is also distinctively different from the 2.72 Å second-nearest O–O distance in aluminum oxide.²⁴

Finally we need to comment on the fact that in Fig. 12(b) peak *B* which is attributed to O–O scattering is larger relative to peak *A* (O–Al scattering) for the $\chi(k)k^3$ than for the $\chi(k)k^2$ Fourier transform. Since the backscattering amplitude $F(k)$ for O ($Z = 8$) falls off faster with increasing k than for Al ($Z = 13$) the $\chi(k)k^3$ transform is expected to increase the weight of peak *A* (O–Al) over peak *B* (O–O) and not vice versa as observed in Fig. 12. We propose that the effect seen in Fig. 12(b) has its origin in an *anisotropic mean free path* of the photoelectron at the surface. As seen from Eq. (3) the total EXAFS amplitude contains a k -dependent term $e^{-2R/\lambda(k)}$, where $\lambda(k)$ is the photoelectron mean free path. For bulk samples $\lambda(k)$ is usually assumed to be isotropic. On surfaces, however, it has to be anisotropic and should in fact be different for scattering directions parallel and perpendicular to the surface. Thus, in our case $\lambda(k)$ may be quite different for the O–O scattering case (parallel to surface only) than for the O–Al one. We note that similar effects also seem to invalidate amplitude transferability from bulk to surface systems as observed for SiO₂ and O on Si(111).⁵⁴

3. 1000-L spectra and oxidized surface

The EXAFS signal $\chi(k)k^3$ for a sample of 1000-L O₂ on Al(111) is shown in Fig. 14. The spectrum was recorded at $\theta = 11^\circ$ after the sample had been heated to 200 °C for 5 min. The Fourier transform of the noisy signal in Fig. 14(a) is shown in Fig. 14(b). It is dominated by a peak *A* around 1.5 Å which we attribute to the O–Al nearest-neighbor distance displaced by a phase shift. Using the phase shift given by Eq. (7) peak *A* corresponds to a distance $R = (1.88 \pm 0.03)$ Å. This distance is about 0.1 Å larger than those obtained for monolayer coverage. We have also reanalyzed our earlier data on a heavily oxidized Al surface²⁴ with the phase shift in Eq. (7). We obtain the same value (1.88 ± 0.03) Å for the O–Al distance as for the 1000-L O₂ spectrum. This distance is slightly different than that derived previously (1.93 Å) using a calculated phase shift.²⁴ Also in our earlier work²⁴ we did not vary Δ in Eq. (2) as should be done according to Lee and Beni⁴⁷ and Martens *et al.*⁴⁸

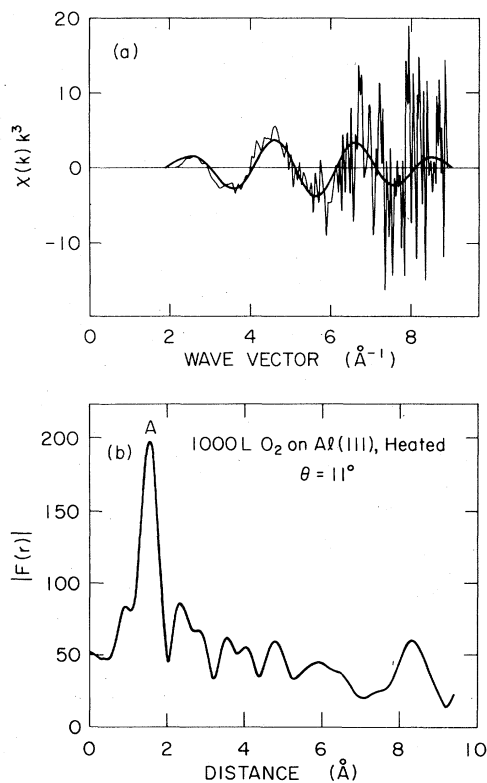


FIG. 14. (a) EXAFS signal $\chi(k)k^3$ for a sample of 1000-L O₂ on Al(111) heated to 200 °C for 5 min, recorded for $\theta = 11^\circ$ (noisy signal). The smooth line is the Fourier filtered signal corresponding to peak *A* in Fig. 14(b). (b) $|F(r)|$ of the noisy signal in Fig. 14(a).

D. Discussion of structural models

Our results on the O *K*-edge fine structure and extended fine structure suggest certain models for the progressive oxidation of Al(111) surfaces. Starting with the spectra taken around monolayer oxygen coverage we find strong support of a (1 × 1) oxygen overlayer configuration suggested previously by LEED.^{14, 16, 20} Our value of (2.90 ± 0.05) Å for the in-plane O–O distance is in excellent agreement with the $a/\sqrt{2} = 2.86$ Å Al–Al separation in the (111) surface plane. The arrangement of the chemisorbed O atoms is shown in Fig. 8(b).

Our present measurements cannot distinguish between the various possible threefold sites on the (111) surface (e.g., between sites *A* and *B*). However, earlier experimental and theoretical results suggest that O chemisorbs in the threefold hollow sites *A* outside the surface. Our value for the O–Al bond length $R = (1.79 \pm 0.05)$ Å corresponding to a value $Z = 0.70(+0.10, -0.15)$ Å above the Al (111) plane then completely determines the structure of the chemisorbed O–Al surface. It is interesting to note that the O atoms are located in positions which are a continuation of the Al lattice (fcc stacking). However, the interplanar distance *Z* is reduced considerably ($Z = 0.70$ Å) relative to the interplanar separation of $a/\sqrt{3} = 2.33$ Å for bulk Al (see Fig. 8).

For the oxide phase which accompanies the chemisorption phase we find the same O–Al bond length within experimental error. This strongly suggests the geometry shown in Fig. 8(c) for this phase. Here an O atom is bonded to four Al atoms as in Al₂O₃ (corundum) and γ -Al₂O₃.²⁶ The ideal O–Al bond length for the shown tetrahedral interstice position is $\frac{1}{4}a\sqrt{3} = 1.75$ Å which is remarkably close to our experimental value (1.79 ± 0.05) Å. The site shown in Fig. 8(c) can be occupied simultaneously with the chemisorption site. As for the chemisorption site the O atoms form a (1 × 1) configuration relative to the clean Al(111) surface. This can explain that a sharp (1 × 1) LEED pattern exists up to relatively high (~1000 L) oxygen exposures corresponding to more than monolayer coverage.

Our results for the O–Al bond length around monolayer oxygen coverage are in conflict with the findings of a recent multiple-scattering LEED analysis. Martinson *et al.*²⁰ deduced a O–Al separation of $R = (2.12 \pm 0.05)$ Å corresponding to $Z = (1.33 \pm 0.08)$ Å for the chemisorbed stage. Their LEED spectra were recorded in the same 100–150-L O₂ exposure range as used here. The large *R* value reported by Martinson *et al.* would be truly exceptional as judged from available O–Al bond lengths in bulk crystals (1.66–1.98 Å),^{52, 55} in the AlO molecule (1.62) (Ref. 55) or from the Slater sum of atomic radii (1.85 Å).⁵⁵ We thus believe the LEED value to be incorrect.

At oxygen exposures where the (1 × 1) LEED spot pattern has disappeared (e.g., 1000 L plus heat) we observe an increased O–Al bond length (1.88 ± 0.03) Å. This is accompanied by the formation of a white-line threshold structure. We attribute this to formation of aluminum oxide which locally resembles the structure of corundum⁵² or γ -Al₂O₃.²⁶ Now the chemisorbed oxygen atoms have also penetrated the surface Al layer and formed bonds with second- and possibly third-layer Al atoms. A larger O–Al bond length results. For example, the site directly underneath the chemisorption site [Fig. 8(d)] would ideally yield an O–Al bond length of $\frac{1}{2}a = 2.02$ Å. Our value of $R = 1.88$ Å is in fact identical to the O–Al separation in the spinel-like γ -Al₂O₃ (Ref. 26) and close to the average O–Al distance 1.915 in corundum Al₂O₃.³¹ By comparison of the bond lengths we conclude that at heavy oxygen coverage a surface oxide forms which has a structure similar to that of γ -Al₂O₃. This was in fact already suggested by Verwey in 1935.⁵⁵

In our model the oxidelike phase always consists of γ -Al₂O₃-like units. However at low coverage the O–Al bond length is reduced because of the constraints placed by the Al lattice [Fig. 8(c)]. At higher coverage (>1000-L O₂) reconstruction of the Al surface atoms occurs and the bond length can now assume the 1.88-Å value found in bulk γ -Al₂O₃. One point which remains to be discussed is that the Al *2p* chemical shift is identical for the oxidelike phase around monolayer coverage [$R_{O-Al} = (1.79 \pm 0.05)$ Å], the disordered oxide phase [$R_{O-Al} = (1.88 \pm 0.03)$ Å] and bulk Al₂O₃ ($R_{O-Al} = 1.915$ Å). This would indicate a very similar total charge transfer from the Al to the neighboring O atoms in all cases. For our model the oxygen coordination *N* of the Al atoms is lower ($N \leq 3$) for the initial oxide phase than for the high coverage phase and Al₂O₃ ($N = 6$). Thus if the total charge transfer from Al is the same in all cases a larger charge transfer per O atom would result for the low coverage oxide. This would result in a shorter bond length as observed.

V. CONCLUSIONS

From analysis of the O *K*-edge fine structure and extended fine structure we have deduced a model for the progressive oxidation of Al(111) surfaces. Using additional information provided by previous studies we have completely determined the structure of the O–Al chemisorption complex. It appears that a consistent picture of the structural and electronic properties of the (1 × 1) oxygen on Al(111) surface does now exist if our results are combined with the photoemission data of Flodström *et al.*¹⁶ and the self-consistent-field *Xα* calculations of Salahub *et al.*⁶ Our results indicate deficiencies in atom-jellium-type

calculations² even when pseudopotentials are included to first order⁹ and also strongly disagree with the conclusions drawn from a recent LEED intensity analysis.²⁰ We also suggest a model for the formation of the oxidelike phase which is characterized by a larger Al 2*p* chemical shift than for the chemisorbed phase. An atomic arrangement is proposed which resembles that in γ -Al₂O₃ where an O atom is surrounded by four equidistant Al atoms.²⁶ As the oxidation progresses reconstruction of the Al atoms near the surface occurs and the O-Al bond length increases. The O *K* edge is found to change significantly with oxygen exposure. This is discussed in terms of formation of aluminum-oxidelike molecular units with increasing oxidation. It is pointed out that this phenomenon may have significant future applications in the study of adsorbate systems. Analysis of

the threshold structure may by itself provide information on the local structure of surface complexes.

ACKNOWLEDGMENTS

We would like to thank I. Lindau and W. E. Spicer for providing the data acquisition system. One of us (J. S.) has greatly benefited from discussions with F. W. Kutzler, d. K. Misemer, and S. Doniach regarding the structure of absorption thresholds. The work at SSRL was supported by the National Science Foundation under Contract No. DMR 77-27489 in cooperation with SLAC and the Basic Energy Division of the Department of Energy and the NSF-MRL Program through the Center for Materials Research at Stanford University.

- ¹For a review see A. W. Smith, Some Basic Principles of Surface Preparation of Aluminum for Adhesive Bonding, Boeing Scientific Research Laboratories Report D1-82-1003 (1970) (unpublished).
- ²N. D. Lang and A. R. Williams, Phys. Rev. Lett. **34**, 531 (1975); Phys. Rev. B **18**, 616 (1978).
- ³J. Harris and G. S. Painter, Phys. Rev. Lett. **36**, 151 (1976); G. S. Painter, Phys. Rev. B **17**, 662 (1978).
- ⁴I. P. Batra and S. Ciraci, Phys. Rev. Lett. **39**, 774 (1977).
- ⁵R. P. Messmer and D. R. Salahub, Chem. Phys. Lett. **49**, 59 (1977); D. R. Salahub and R. P. Messmer, Phys. Rev. B **16**, 2526 (1977); R. P. Messmer and D. R. Salahub, *ibid.* **16**, 3415 (1977).
- ⁶D. R. Salahub, M. Roche, and R. P. Messmer, Phys. Rev. B **18**, 6495 (1978).
- ⁷L. I. Johansson and J. Stöhr, Phys. Rev. Lett. **43**, 1882 (1979).
- ⁸S. A. Flodström, R. Z. Bachrach, R. S. Bauer, and S. B. M. Hagström, Phys. Rev. Lett. **37**, 1282 (1976).
- ⁹K. Y. Yu, J. N. Miller, P. Chye, W. E. Spicer, N. D. Lang, and A. R. Williams, Phys. Rev. B **14**, 1446 (1976).
- ¹⁰S. A. Flodström, L.-G. Petersson, and S. B. M. Hagström, J. Vac. Sci. Technol. **13**, 280 (1976).
- ¹¹S. A. Flodström, L.-G. Petersson, and S. B. M. Hagström, Solid State Commun. **19**, 257 (1976).
- ¹²D. Norman and D. P. Woodruff, J. Vac. Sci. Technol. **15**, 1580 (1978).
- ¹³W. Eberhardt and C. Kunz, Surf. Sci. **75**, 709 (1978).
- ¹⁴R. Payling and J. A. Ramsay, Proceedings of the 5th Australian Vacuum Conference, Brisbane, 1976 (unpublished), p.131.
- ¹⁵P. O. Gartland, Surf. Sci. **62**, 183 (1977).
- ¹⁶S. A. Flodström, C. W. B. Martinson, R. Z. Bachrach, S. B. M. Hagström, and R. S. Bauer, Phys. Rev. Lett. **40**, 907 (1978).
- ¹⁷P. Hofmann, W. Wyrobisch, and A. M. Bradshaw, Surf. Sci. **80**, 344 (1979).
- ¹⁸W. Eberhardt and F. J. Himpsel, Phys. Rev. Lett. **42**, 1375 (1979).
- ¹⁹C. W. B. Martinson and S. A. Flodström, Solid State Commun. **30**, 671 (1979).
- ²⁰C. W. B. Martinson, S. A. Flodström, J. Rundgren, and P. Westrin, Surf. Sci. **89**, 102 (1979).
- ²¹A. Barrie, Chem. Phys. Lett. **19**, 109 (1973).
- ²²For examples see J. B. Pendry, *Low Energy Electron Diffraction* (Academic, New York, 1974); C. B. Duke, in *Surface Effects in Crystal Plasticity*, edited by R. M. La Tansion and J. F. Fourie (Noordhoff, Leyden, 1977), p. 165-219; S. Y. Tong, in *Electron Diffraction 1927-1977*, edited by P. J. Dobson *et al.* (Institute of Physics, London, 1977), pp. 270-280; F. Jona, J. Phys. C **11**, 4271 (1978).
- ²³P. H. Citrin, P. Eisenberger, and R. C. Hewitt, Phys. Rev. Lett. **44**, 309 (1978).
- ²⁴J. Stöhr, D. Denley, and P. Perfetti, Phys. Rev. B **18**, 4132 (1978).
- ²⁵A. Bianconi and R. Z. Bachrach, Phys. Rev. Lett. **42**, 104 (1979).
- ²⁶E. Kordes, Z. Kristallogr. **91**, 193 (1935); G. Hägg and G. Söderholm, Z. Phys. Chem. Abt. B **29**, 88 (1935); E. J. W. Verwey, Z. Kristallogr. **91**, 65 (1935).
- ²⁷J. L. Dehmer, J. Chem. Phys. **56**, 4496 (1972).
- ²⁸J. L. Dehmer and D. Dill, J. Chem. Phys. **65**, 6327 (1976).
- ²⁹J. Stöhr, L. I. Johansson, I. Lindau, and P. Pianetta, Phys. Rev. B **20**, 664 (1979).
- ³⁰F. C. Brown, R. Z. Bachrach, S. B. M. Hagström, N. Lien, and C. H. Pruett, in *Vacuum Ultraviolet Radiation Physics*, edited by E. E. Koch, R. Haensel, and C. Kunz (Pergamon, Vieweg, 1974), p. 785; F. C. Brown, R. Z. Bachrach, and N. Lien, Nucl. Instrum. Methods **152**, 73 (1978).
- ³¹For a convenient listing of bond lengths, see J. C. Slater, *Symmetry and Energy Bands in Crystals* (Dover, New York, 1972), pp. 308-346.
- ³²P. W. Palmberg, J. Electron Spectrosc. Relat. Phenom. **5**, 691 (1974).
- ³³J. Stöhr and D. Denley, in Proceedings of the International Workshop on X-ray Instrumentation for Synchrotron Radiation, edited by H. Winick and G. S. Brown, Stanford, SSRL Report 78/04, 1978 (unpublished).
- ³⁴J. Stöhr, J. Vac. Sci. Technol. **16**, 37 (1979).
- ³⁵G. Martens, P. Rabe, N. Schwentner, and A. Werner, J.

- Phys. C 11, 3125 (1978).
- ³⁶J. Stöhr, Jpn. J. Appl. Phys. Suppl. 17-2, 217 (1978).
- ³⁷J. Stöhr, R. S. Bauer, J. C. McMenamin, L. I. Johansson, and S. Brennan, J. Vac. Sci. Technol. 16, 1195 (1979).
- ³⁸For a review see A. Kotani and Y. Toyozawa, in *Synchrotron Radiation, Techniques and Applications*, edited by C. Kunz (Springer, Berlin, 1979), p. 169.
- ³⁹F. W. Lytle, J. Catal. 43, 376 (1976).
- ⁴⁰M. Brown, R. E. Peierls, and E. A. Stern, Phys. Rev. B 15, 738 (1977); S. M. Heald and E. A. Stern, *ibid.* 16, 5549 (1977).
- ⁴¹D. Denley, R. S. Williams, P. Perfetti, D. A. Shirley, and J. Stöhr, Phys. Rev. B 19, 1762 (1979).
- ⁴²C. R. Natoli, F. W. Kutzler, D. K. Misemer, and S. Doniach, Phys. Rev. A 22, 1104 (1980).
- ⁴³A. Bianconi, R. Z. Bachrach, and S. A. Flodström, Phys. Rev. B 19, 3879 (1979).
- ⁴⁴C. Senemaud and M. T. Costa Lima, J. Phys. Chem. Solids 37, 83 (1976).
- ⁴⁵D. E. Sayers, F. W. Lytle, and E. A. Stern, Phys. Rev. Lett. 27, 1204 (1971).
- ⁴⁶E. A. Stern, Phys. Rev. B 10, 3027 (1974); C. H. Ashley and S. Doniach, *ibid.* 11, 1279 (1975); P. A. Lee and J. B. Pendry, *ibid.* 11, 2795 (1975).
- ⁴⁷P. A. Lee and G. Beni, Phys. Rev. B 15, 2862 (1977).
- ⁴⁸G. Martens, P. Rabe, N. Schwentner, and A. Werner, Phys. Rev. B 17, 1418 (1978).
- ⁴⁹P. A. Lee, Phys. Rev. B 13, 5261 (1976).
- ⁵⁰E. A. Stern, D. E. Sayers, J. G. Dash, H. Shechter, and B. Bunker, Phys. Rev. Lett. 38, 767 (1977); S. M. Heald and E. A. Stern, Phys. Rev. B 17, 4069 (1978).
- ⁵¹G. S. Brown, P. Eisenberger, and P. Schmidt, Solid State Commun. 24, 201 (1977).
- ⁵²R. W. G. Wyckoff, *Crystal Structures* (Wiley, New York, 1964); A. F. Wells, *Structural Inorganic Chemistry* (Oxford University Press, New York, 1975).
- ⁵³P. A. Lee, Boon-Keng Teo, and A. L. Simmons, J. Am. Chem. Soc. 99, 3856 (1977); Boon-Keng Teo and P. A. Lee, *ibid.* 101, 2815 (1979).
- ⁵⁴J. Stöhr, L. I. Johansson, I. Lindau, and P. Pianetta, J. Vac. Sci. Technol. 16, 1221 (1979).
- ⁵⁵E. J. W. Verwey, Z. Kristallogr. 91, 317 (1935).